UNSTRUCTURED GRIDS AND AN ELEMENT BASED CONSERVATIVE APPROACH FOR A BLACK-OIL RESERVOIR SIMULATION

Régis Lopes Nogueira, regisln@uol.com.br
Bruno Ramon Batista Fernandes, brbfernandes@yahoo.com.br
Federal University of Ceará, Fortaleza, Ceará, Brazil
Department of Chemical Engineering

André Luiz de Souza Araújo, andre@ifce.edu.br
Federal Institution of Education, Science and Technology of Ceará – IFCE
Industry Department

Francisco Marcondes, marcondes@ufc.br
Federal University of Ceará, Fortaleza, Ceará, Brazil
Department of Metallurgical Engineering and Material Science

Abstract. *Unstructured meshes presented one upgrade in modeling the main important features of the reservoir such as discrete fractures, faults, and irregular boundaries. From several methodologies available, the Element based Finite Volume Method (EbFVM), in conjunction with unstructured meshes, is one methodology that deserves large attention. In this approach, the reservoir, for 2D domains, is discretized using a mixed two-dimensional mesh using quadrilateral and triangle elements. After the initial step of discretization, each element is divided into sub-elements and the mass balance for each component is developed for each sub-element. The equations for each control-volume using a cell vertex construction are formulated through the contribution of different neighbored elements. This paper presents an investigation of an element-based approach using the black-oil model based on pressure and global mass fractions. In this approach, even when all gas phase is dissolved in oil phase the global mass fraction of gas will be different from zero. Therefore, no additional numerical procedure is necessary in order to treat the gas phase appear/disappearance. In this paper the above mentioned approach is applied to multiphase flows involving oil, gas, and water. The mass balance equations in terms of global mass fraction of oil, gas and water are discretized through the EbFVM and linearized by the Newton's method. The results are presented in terms of volumetric rates of oil, gas, and water and phase saturations.*

Keywords*: Black-oil model, Global mass fractions, EbFVM, Multiphase flow.*

1. INTRODUCTION

Unstructured mesh is one important tool for modeling important features of the reservoirs such as discrete fractures, faults, and irregular boundaries, and as well deviated wells. From several options available, the EbFVM is one methodology that has received a lot of attention in the literature (Cordazzo, 2004; Cordazzo et al. 2004a-b; Marcondes and Sepehrnoori, 2007; Karpinski et al. 2009; Marcondes and Sepehrnoori, 2010), mainly because is locally conservative. In this paper, this EbFVM approach is applied to the black-oil model in terms of Global mass fraction and pressure (Maliska et al., 1997; Prais and Campagnolo, 1981; Nunes et al., 2009) for simulating three phase flow (oil, gas, and water).

The EbFVM approach combines the flexibility obtained by the Finite Element Method with the property of locally and globally conservation from the classical Finite Volume Method. It employs the ideas of Baliga and Patankar (1988), and Raw (1985) to develop the method of FIELDS to solve the Navier-Stokes equations. In the literature, this method is generally known as the Control Volume Finite Element Method (CVFEM). However, a better denomination would be Element based Finite Volume Element Method (EbFVM) as defined by Maliska (2004), since this approach is still a finite volume method, which only borrows, from the finite element technique, the concept of elements and their functions. On the other hand, CVFEM erroneously suggest a finite element formulation that meets the conservation principles at the discrete level. Therefore, the name EbFVM will be used throughout this paper.

This paper proposes a methodology for numerical simulation of multiphase flow using the black-oil model in conjunction with the EbFVM approach and unstructured meshes using quadrilateral and triangles. The black-oil model considers the system with only three components - oil, water and gas - and three phases, also known as oil, water and gas. It is assumed that the component oil and water only exist in the oil and water phase, respectively, and the gas component can be found either in the gas phase or in oil phase. This model also considers that the temperature of the reservoir is constant and that there are no chemical reactions between components. This model is recommended for heavy oils with low volatility, like those ones found in Brazil (Cordazzo, 2006).The mass balance equations in terms of global mass fraction of oil, gas and water are discretized through the finite-volume method and linearized by the Newton's method. The results are presented in terms of volumetric rates of oil, gas, and water, and as well as phase saturation fields.

2. PHYSICAL MODEL

The black-oil equations for the water, oil, and gas components in terms of the global mass fractions and pressures are given by:

$$\frac{\partial}{\partial t}\left(\phi\rho_m Z_w\right) = \vec{\nabla}.\left(\lambda_w \bar{\bar{K}}.\vec{\nabla}\Phi_w\right) - \bar{m}_w, \tag{1}$$

$$\frac{\partial}{\partial t}\left(\phi\rho_m Z_o\right) = \vec{\nabla}.\left(X_{oo}\lambda_o \bar{\bar{K}}.\vec{\nabla}\Phi_o\right) - X_{oo}\bar{m}_o, \tag{2}$$

$$\frac{\partial}{\partial t}\left(\phi\rho_m Z_g\right) = \vec{\nabla}.\left((1-X_{oo})\lambda_o \bar{\bar{K}}.\vec{\nabla}\Phi_o + \lambda_g \bar{\bar{K}}.\vec{\nabla}\Phi_g\right) - (1-X_{oo})\bar{m}_o - \bar{m}_g. \tag{3}$$

By summing Eqs. (1)-(3), the following global mass conservation equation is obtained:

$$\frac{\partial}{\partial t}\left(\phi\rho_m\right) = \vec{\nabla}.\left(\lambda_w \bar{\bar{K}}.\vec{\nabla}\Phi_w + \lambda_o \bar{\bar{K}}.\vec{\nabla}\Phi_o + \lambda_g \bar{\bar{K}}.\vec{\nabla}\Phi_g\right) - \bar{m}_w - \bar{m}_o - \bar{m}_g. \tag{4}$$

In this work, Eq. (4), is called pressure equation. In Eqs. (1) through (4), ϕ denotes the porosity, ρ_m denotes the average density, Z_w, Z_o, Z_g are the water, oil, and gas global mass fractions, respectively, X_{oo} denotes the mass fraction of component oil in oil phase, λ_w, λ_o, λ_g are mobilities of the water, oil, and gas phases, respectively, multiplied by the density of the each phase, $\bar{m}_w$, $\bar{m}_o$, $\bar{m}_g$ are the mass flow rate of water, oil and gas phases, respectively per unit of bulk volume of the reservoir. These terms represent the sink or source terms for the control volumes which could contain a well. K is the absolute permeability tensor which is assumed, in this work, as a diagonal tensor. The potential of each phase (Φ) is given by

$$\Phi_p = P_p - \rho_p g\, z, \tag{5}$$

where p denotes the water, oil, or gas phase, P is the pressure, ρ_p is the density of phase p, g is gravity, and z is the depth, which is positive in the upward direction. Inspecting Eqs. (1) through (5), we can be inferred that there are 6 unknowns (Z_w, Z_o, Z_g, P_w, P_o, and P_g) and only three equations, since Eq. (4) is just a combination of Eqs. (1)-(3). The closing equations comes from capillarity pressure relations and the mass conservation equation which requires

$$Z_w + Z_o + Z_g = 1 \tag{6}$$

The problem under consideration is a multiphase flow in porous media. For reasons of simplicity, some effects are neglected in this work: chemical reactions, thermal effects and capillary.

3. APPROXIMATE EQUATIONS

In order to obtain the approximate equation for each component, the conservation equations need to be integrated in time and for each sub-control volume shown in Fig. 1. Considering the Eqs. (1)-(3), for a generic component p, the following equation is obtained:

$$\int_{V,t}\frac{\partial}{\partial t}\left(\phi\rho_m Z_p\right)dVdt = \int_{V,t}\vec{\nabla}.\left(\lambda_p \bar{\bar{K}}.\vec{\nabla}\Phi_p\right)dVdt - \int_{V,t}\bar{m}_p dVdt. \tag{7}$$

Applying the Gauss theorem to the first term in the right-had side of Eq. 7, one obtains:

$$\int_{V,t}\frac{\partial}{\partial t}\left(\phi\rho_m Z_p\right)dVdt = \int_{S,t}\left(\lambda_p \bar{\bar{K}}.\vec{\nabla}\Phi_p\right)dSdt - \int_{V,t}\bar{m}_p dVdt. \tag{8}$$

By performing the time integrations and dividing the right-hand side terms by the time step (Δt), we obtain the following equation:

$$\sum_{i}^{NEl}\left(\frac{\left(\phi\rho_m Z_p\right)-\left(\phi\rho_m Z_p\right)^0}{\Delta t}\right)_i V_{SCv_i}=\int_S\left(\lambda_p\bar{\bar{K}}.\vec{\nabla}\Phi_p\right).\overrightarrow{dS}-\bar{m}_p, \tag{9}$$

where the surface integral is performed over all edges of each sub-control volume. No matter the element shape, there are two integration points where integral surface needs to be evaluated (see Fig. 1). In order to evaluate the first term in the right-hand side of Eq. (9), it is necessary to define the shape functions. The shape functions, for triangular and quadrilateral elements are respectively, given by

$$N_1(\xi,\eta)=1-\xi-\eta\ ;\ N_2(\xi,\eta)=\xi\ ;\ N_3(\xi,\eta)=\eta\ , \tag{10}$$

$$N_1(\xi,\eta)=\frac{1}{4}(1+\xi)(1+\eta)\ ;\ N_2(\xi,\eta)=\frac{1}{4}(1-\xi)(1+\eta)\ ;\ N_3(\xi,\eta)=\frac{1}{4}(1-\xi)(1-\eta)\ ;\ N_4(\xi,\eta)=\frac{1}{4}(1+\xi)(1-\eta)\ , \tag{11}$$

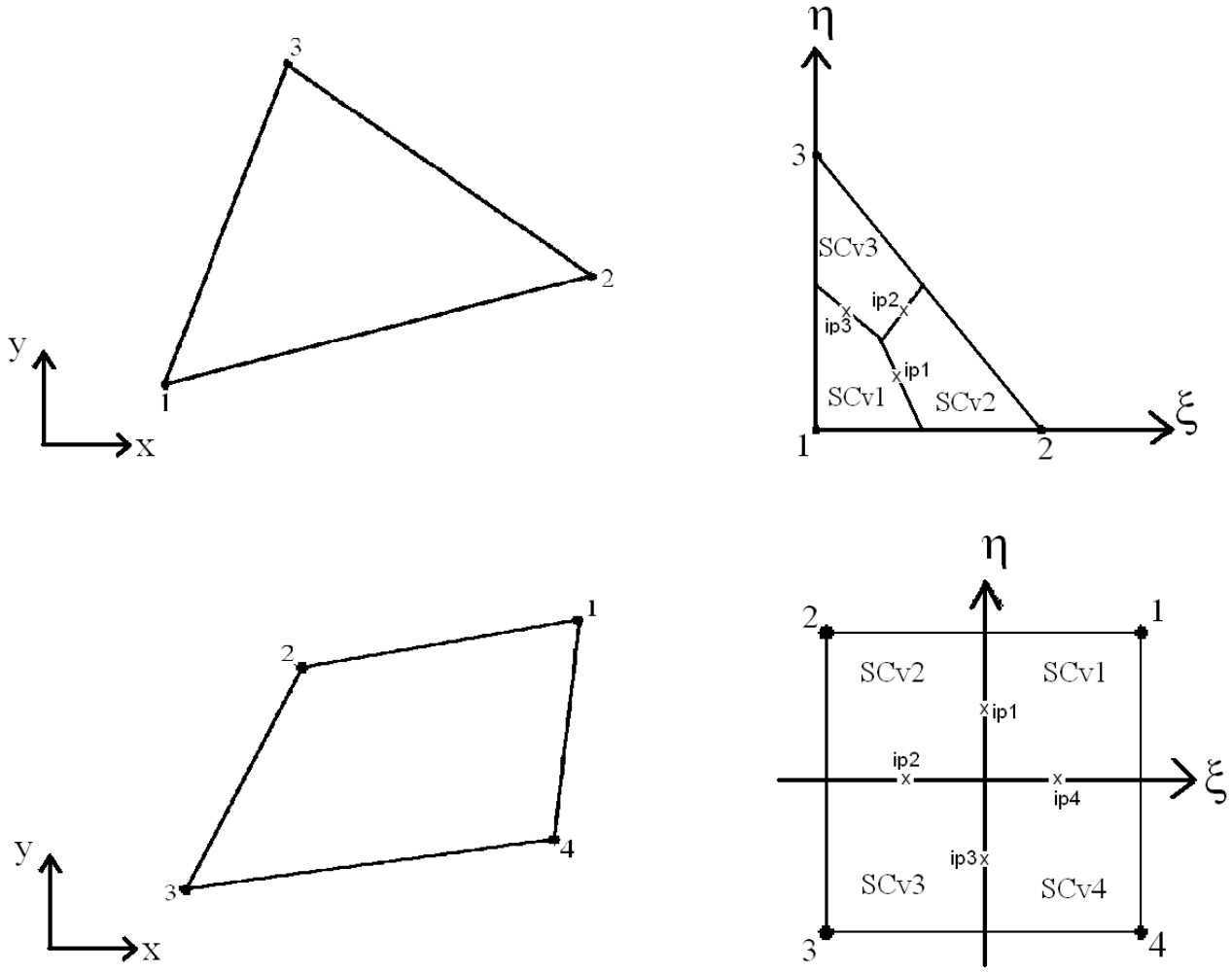

Figure 1. Triangular and quadrilateral elements, and its respective sub-control volumes (*SCV*).

By using the shape functions any physical properties or positions can be evaluated inside an element as

$$p(\xi,\eta)=\sum_{i=1}^{NNE}N_i(\xi,\eta)P_i\ ;\ x(\xi,\eta)=\sum_{i=1}^{NNE}N_i(\xi,\eta)X_i\ ;\ y(\xi,\eta)=\sum_{i=1}^{NNE}N_i(\xi,\eta)Y_i\ , \tag{12}$$

where NNE denotes the number of vertex for each element. Elements using the same shape function for coordinates and physical properties are known as isoparametric elements (Hughes, 1987). Using the shape functions, gradients of potentials can be easily evaluated as

$$\frac{\partial p}{\partial x} = \sum_{i=1}^{NNE} \frac{\partial N_i}{\partial x} P_i \; ; \; \frac{\partial p}{\partial y} = \sum_{i=1}^{NNE} \frac{\partial N_i}{\partial y} P_i \; . \tag{13}$$

To evaluate the gradients, it is necessary to obtain the derivatives of shape functions relative to x and y. These derivatives are given by

$$\frac{\partial N_i}{\partial x} = \frac{1}{\det(J_t)} \left(\frac{\partial N_i}{\partial \xi} \frac{\partial y}{\partial \eta} - \frac{\partial N_i}{\partial \eta} \frac{\partial y}{\partial \xi} \right) ; \; \frac{\partial N_i}{\partial y} = \frac{1}{\det(J_t)} \left(\frac{\partial N_i}{\partial \eta} \frac{\partial x}{\partial \xi} - \frac{\partial N_i}{\partial \xi} \frac{\partial x}{\partial \eta} \right) , \tag{14}$$

where J_t is the Jacobian of the transformation and it is given by

$$\det(J_t) = \left(\frac{\partial x}{\partial \xi} \frac{\partial y}{\partial \eta} - \frac{\partial x}{\partial \eta} \frac{\partial y}{\partial \xi} \right) . \tag{15}$$

To perform the first integral in the left and right-hand size of Eq. (9), it is necessary to define the volumes of each sub-control volume and the areas of each interface. The volumes of each sub-control for triangles and quadrilaterals, respectively, are given by:

$$V_{SVC_i} = \frac{\det(J_t) h}{6} , \tag{16}$$

$$V_{SVC_i} = \det(J_t) h , \tag{17}$$

where h is the thickness of the reservoir. For quadrilateral *det(Jt)* needs to be evaluated at the center of each sub-control volume. The area of each interface, reading a counterclockwise, is given by

$$d\vec{S} = h dy \hat{i} - h dx \hat{j} . \tag{18}$$

By using a midpoint approximation along each integration point in Eq. (9), results in the following equation for each sub-control volume:

$$\sum_{i=1}^{NNE} \left[\frac{\left(\phi \rho_m Z_p \right)_i - \left(\phi \rho_m Z_p \right)_i^0}{\Delta t} \right] V_{SCV_i} = \sum_{i}^{NNE} \left(\lambda_p \overline{\overline{K}} \vec{\nabla} \Phi_p . \overrightarrow{\Delta S} \right)_i - \overline{m}_p . \tag{19}$$

By substituting Eqs. (16) and (17) for the accumulation term, and Eq. (18) for the advective flux into Eq. (19), and evaluating the fluid properties through a fully implicit procedure the following equations for the two mentioned terms are obtained:

$$Acc = \sum_{i=1}^{NNE} \left[\frac{\left(\phi \rho_m Z_p \right)_i - \left(\phi \rho_m Z_p \right)_i^0}{\Delta t} \right] V_{SCV_i} , \tag{20}$$

$$F_{m,i} = \sum_{i}^{NNE} \left(\lambda_p \overline{\overline{K}} \vec{\nabla} \Phi_p . \overrightarrow{\Delta S} \right)_i . \tag{21}$$

By inspecting Eq. (21), it can be inferred that it is necessary to evaluate mass densities, mass fraction and mobilities in two interfaces of each sub-control volume. To evaluate these properties, an upwind scheme based on Cordazzo (2004) will be used. The mobilities and other fluid properties are evaluated at the integration point 1 of Fig. 1, for instance, by

$$\lambda_{jk} = \lambda_j \text{ if } \left(\overline{\overline{K}} \vec{\nabla} \Phi_j . d\vec{S} \right)_{ip1} \le 0 \; ; \; \lambda_{jk} = \lambda_k \text{ if } \left(\overline{\overline{K}} \vec{\nabla} \Phi_j . d\vec{S} \right)_{ip1} > 0 , \qquad . \tag{22}$$

where the node *j* considered in the above equations is correspondent to the sub-control volume whereby the normal vector associated to ΔS points outward. Note that this scheme is based on the evaluation of the flow direction, even though the mobility term was omitted in Eq. (10), because it yields always a positive value. The scheme outlined in Eq. (22) assures that the mobilities that will be used at the interfaces are the ones located on the upstream direction, even in cases where the medium is anisotropic. Differently from the classical finite volume method where elements and control volumes are coincident (cell centered construction), in the EbFVM approach control volumes are built around grid nodes, joining the center of the elements to its medians (cell vertex construction). The resulting control volume is formed by portions (sub-control volumes) of neighboring elements, as shown in Fig. 1. Equation (19) represents the conservation equation for each sub-control volume of each element. Now, it is necessary to assemble the equation of each control volume obtaining the contribution of each sub-control volume that shares the same vertex.

4. TEST PROBLEMS

In order to show the application of the methodology employed in the present work four case studies were carried out. The first one is the simulation of a square undersaturated reservoir with a producer well in its center. Table 1 presents the fluid and physical properties. The relative permeability curves for the all case all studies shown in this paper are given in Tabs. 2 and 3. Also, the capillary pressure was set to zero for all simulated case studies.

Table 1 – Input data for case 1.

Reservoir data	Initial condition	Physical properties	Well conditions
$K = 9.9 \times 10^{-13}$ m^3 $A = 2.1404 \times 10^6$ m^2 h = 15m $\phi = 0.2$ $c_r = 0.0$ $r_w = 0.122$ m	$P = 20 \times 10^6$ Pa $S_{wi} = 0.12$ $S_{oi} = 0.88$	$B_w = 1$ at 0 Pa $c_w = 1.00 \times 10^{-10}$ Pa^{-1} $c_o = 1.985 \times 10^{-9}$ Pa^{-1}	$P_{wf} = 20 \times 10^6$ Pa

Table 2 – Oil-gas relative permeability as a function of liquid saturation (S_w+S_o).

S_{lt}	k_{rg}	k_{rog}
0.00000	0.984	0.0000
0.03409	0.980	0.0000
0.20454	0.940	0.0000
0.31818	0.870	0.0004
0.43182	0.720	0.0010
0.48864	0.600	0.0100
0.54545	0.410	0.0210
0.65909	0.190	0.0900
0.71591	0.125	0.2000
0.77273	0.075	0.3500
0.86364	0.025	0.7000
0.94318	0.005	0.9800
0.97727	0.000	0.9970
0.99886	0.000	1.0000

Table 3 – oil-water relative permeability as a function of water saturation (S_w).

S_w	K_{rw}	K_{ro}
0.12	0.00	1.00
0.82	1.00	0.00

The second and third case studies refer to a simulation in a saturated quarter of five spot, but water is injected in the former second case study, and gas is injected for the latter one. Figure 2 shows the unstructured meshes employed for case study one, two and three.

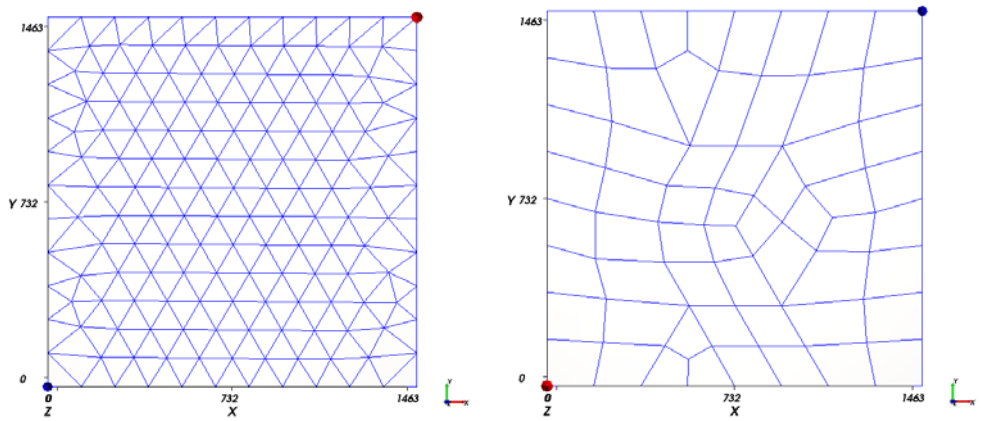

Figure 2. Unstructured meshes. a) Triangular mesh with 162 vertices; b) Quadrilateral mesh with 75 vertices.

Table 4 presents the fluid and physical properties for case studies 2 and 3, where q_i denotes the injected volumetric rate of water or gas.

Table 4 – Input data for case 2 and 3.

Reservoir data	Initial condition	Physical properties	Well conditions
$K = 9.9 \times 10^{-13}$ m^3 $A = 2.1404 \times 10^{6}$ m^2 h = 15m $\phi = 0.2$ $c_r = 0.0$ $r_w = 0.122$ m	$P = 20 \times 10^{6}$ Pa $S_{wi} = 0.12$ $S_{oi} = 0.88$	$B_w = 1$ at 0 Pa $c_w = 1.00 \times 10^{-10}$ Pa^{-1} $c_o = 1.985 \times 10^{-9}$ Pa^{-1}	$q_i = 17280$ m^3/d $P_{wf} = 20 \times 10^{6}$ Pa

The case study 4 is used to demonstrate the applicability of EbFVM approach to represent complex geometries. For this case, water is also injected in an undersaturated reservoir. Figure 3 shows a hybrid mesh composed of quadrilateral and triangular elements employed for this case study. The input data for this case is presented in Table 5.

Table 5 – Input data for case 4.

Reservoir data	Initial condition	Physical properties	Well conditions
$K = 9.9 \times 10^{-13}$ m^3 $A = 2.2631 \times 10^{6}$ m^2 h = 15m $\phi = 0.2$ $c_r = 0.0$ $r_w = 0.122$ m	$P = 20 \times 10^{6}$ Pa $S_{wi} = 0.12$ $S_{oi} = 0.88$	$B_w = 1$ at 0 Pa $c_w = 1.00 \times 10^{-10}$ Pa^{-1} $c_o = 1.985 \times 10^{-9}$ Pa^{-1}	$q_{wi} = 17280$ m^3/d $P_{wf} = 20 \times 10^{6}$ Pa

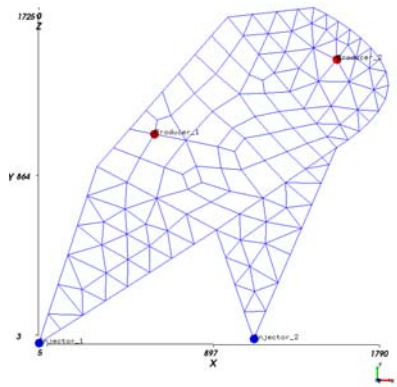

Figure 3. Hybrid mesh used for case 4 with 134 vertices.

5. RESULTS AND DISCUSSIONS

Figure 4 shows the gas saturation field at 39 days for case study 1. From this figure, it possible to verify that after the reservoir depletion gas that was initially miscible with the oil phase appears as free gas into the reservoir demonstrating the ability of black-oil model in terms of global mass fraction to deal with gas the gas phase appearing. Figure 5 presents the oil and gas volumetric flow rates at surface conditions. From that figure, it is possible to infer that results obtained with the triangular and quadrilateral elements were in good agreement. Also, these results are in good agreement with the ones obtained with a 10x10 Cartesian mesh using an in-house simulator. Finally, we can observe that after the initial depletion the volumetric rates of gas and oil become null. This fact happens due to pressure equalization inside the reservoir.

Figure 5 shows the water saturation field for case study 2 at 210 days. Although, it was employed two very coarse meshes the saturation front are approximately the same.

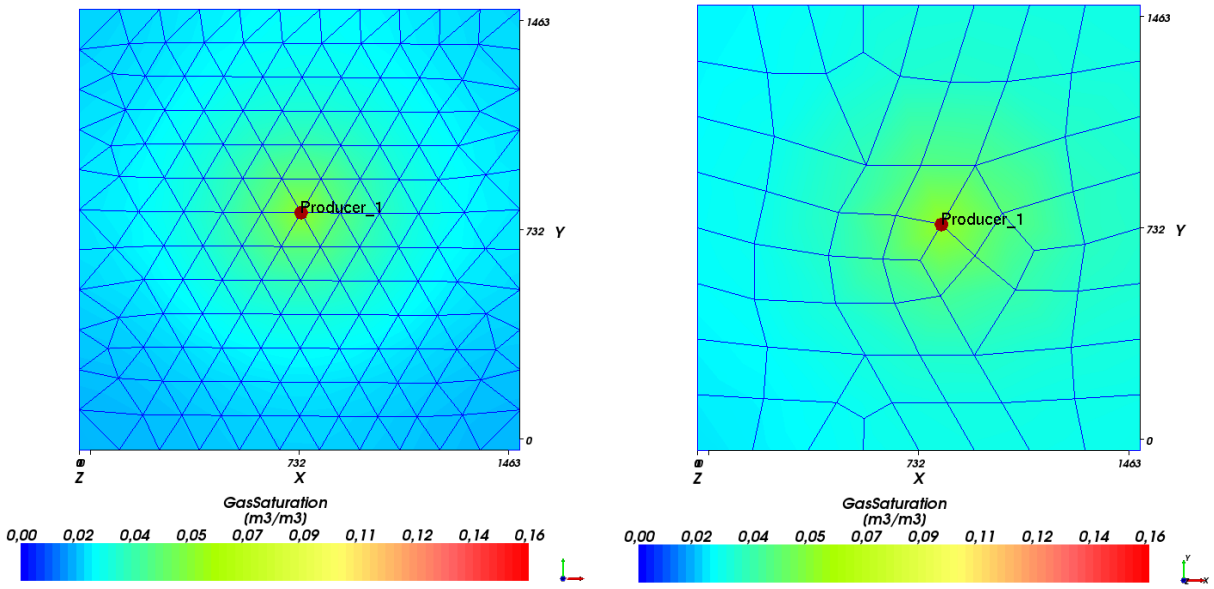

Figure 4. Gas saturation field for case study 1 at 39 days. a) Triangular mesh with 162 vertices; b) Quadrilateral mesh with 75 vertices.

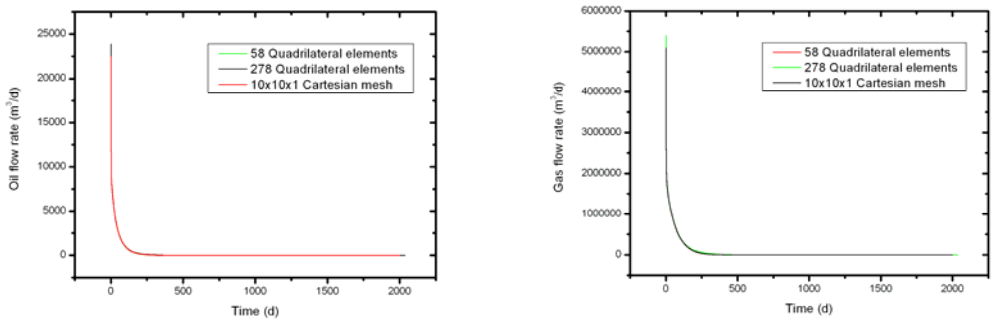

Figure 5. Standard volumetric rates for case 1. a) Oil; b) Gas.

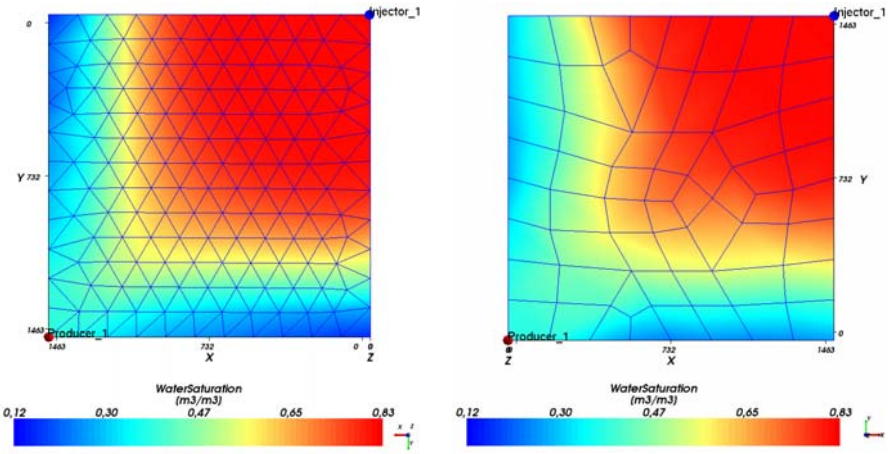

(a) (b)

Figure 6. Water saturation field for case study 2 at 210 days. a) Triangular mesh with 162 vertices; b) Triangular mesh with 75 vertices.

Figure 7 presents oil and water volumetric rates recoveries curves for case study 2 using the meshes presented in Fig. 2, as well as the results using a 10x10 Cartesian mesh. It is important to mention that the volumetric rate of gas showed in Fig. 7b, comes only from the standard gas that was previously miscible with the oil phase at reservoir conditions. Although the volumetric rates were obtained with very coarse meshes, a very good agreement between the volumetric rates was observed. The results were also in good agreement with the ones obtained with the Cartesian mesh.

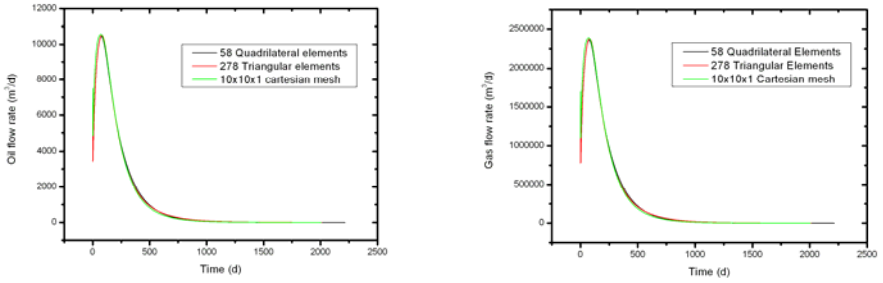

(a) (b)

Figure 7. Transient flow rate for case 2. a) Oil; b) Gas.

Figure 8 shows the gas saturation field for case study 3. Again, the gas saturation fields obtained with both meshes are very close to each other. Although the quadrilateral mesh is very coarse, both field are almost symmetrical.

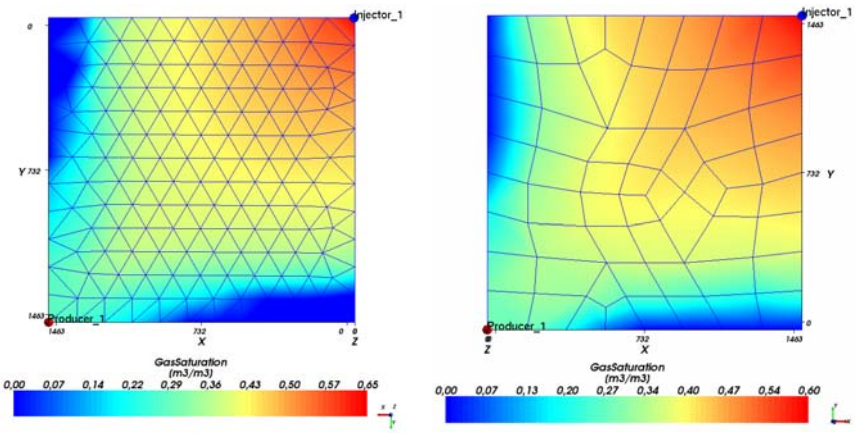

(a) (b)

Figure 8. Gas saturation field for case study 3 at 210 days a) Triangular mesh with 162 vertices; b) Quadrilateral mesh with 75 vertices.

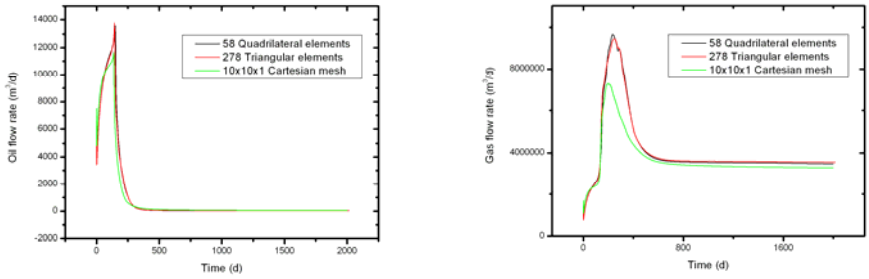

(a) (b)

Figure 9. Transient flow rate for case 3. a) Oil; b) Gas.

Figure 9 presents the volumetric rates of oil and gas at standard conditions. Again the volumetric rates obtained with both meshes are very close to each other. On the other hand, the results obtained with the Cartesian mesh were not close to the ones obtained with EbFVM approach when large variation in volumetric rates occurred.

Figures 10 and 11 present the water saturation field at 41 and 210 days, and oil and gas volumetric rates at standard condition, respectively. Although, the mesh is much distorted the saturation field presented in Fig. 10 is physically acceptable. Once again, the gas volumetric rate presented in Fig. 11b comes from gas the was miscible with the oil phase at the reservoir conditions.

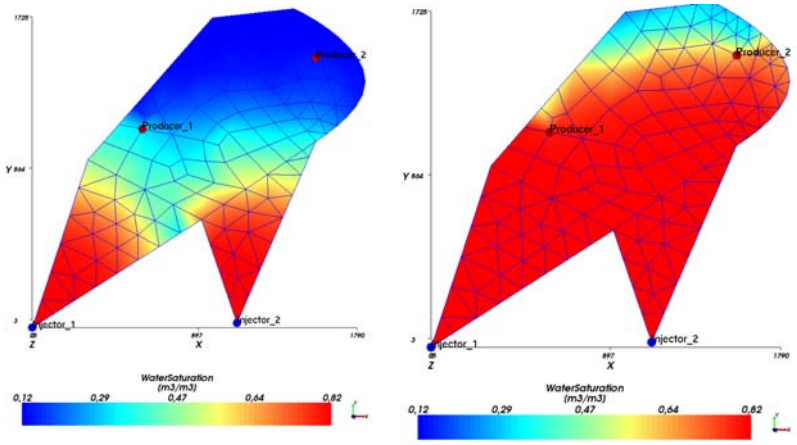

(a) (b)

Figure 10. Water saturation field for case study 4. a) 41 days; b) 210 days.

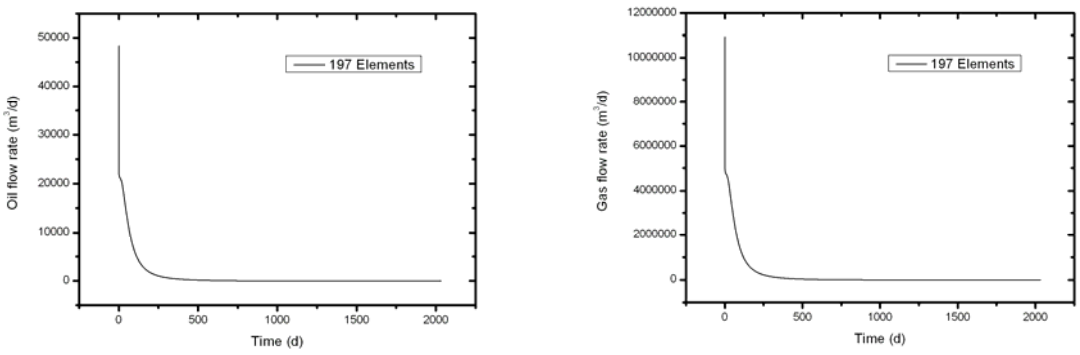

(a) (b)

Figure 11. Transient flow rate for case study 4. a) Oil; b) Gas.

4. CONCLUSIONS

This paper presented an element-based approach for black-oil model in terms of pressure and global mass fraction in conjunction with unstructured meshes. The results for water and gas flooding as well as primary recovery were compared with an in-house simulator using Cartesian meshes. Triangular, quadrangular and hybrid meshes were used for testing and verifications of the implemented approach. The results in terms of volumetric rates of oil, gas, and were in good agreement with the ones obtained with Cartesian meshes.

5. ACKNOWLEDGEMENTS

The authors acknowledge the CNPQ and the Federal University of Ceará for the financial aid.

6. REFERENCES

BALIGA, B.R.; Patankar, S.V., 1980, "A New Finite Element Formulation for Convection Diffusion Problems", Numerical Heat Transfer, Vol. 3, pp. 393-409.

CORDAZZO, J. Simulação de reservatórios de petróleo utilizando o método EbFVM e multigrid algébrico. 2006. Tese (Doutorado em Engenharia Mecânica) – Programa de Pós-Graduação em Engenharia Mecânica. UFSC, Florianópolis. 2006.

CORDAZZO, J., 2004, An Element Based Conservative Scheme using Unstructured Grids for Reservoir Simulation, SPE International Student Paper Contest, The SPE Annual Technical Conference and Exhibition, Houston, Texas.

CORDAZZO, J., Maliska, C. R., Silva, A. F. C., and Hurtado, F. S. V., 2004, The Negative Transmissibility Issue When Using CVFEM in Petroleum Reservoir Simulation - 1. Theory", The 10th Brazilian Congress of Thermal Sciences and Engineering - ENCIT 2004, Braz. Soc. of Mechanical Sciences and Engineering - ABCM, Rio de Janeiro, Brazil, Nov. 29-Dec. 03.

HUGHES, T.J.R., The Finite Element Method, Linear Static and Dynamic Finite Element Analysis. Prentice Hall, New Jersey. 1987.

KARPINSK, L., Maliska, C.R., Marcondes, F. Delshad, M., and Sephrnoori, K., 2009, An Element Based Conservative Approach Using Unstructured Grids in Conjunction with a Chemical Fooding Compositional Reservoir Simulator, 20th International Congress of Mechanical Engineering, Gramado, RS.

MALISKA, C. R., 2004, Heat Transfer and Computational Fluid Mechanics, Florianópolis, 2ª. Ed. Editora LTC. (In Portuguese).

MALISKA, C.R., da Silva, A.F.C., Czesnat, A.O., Lucianetti, R.M., and Maliska Jr., C.R., 1997, "Three-Dimensional Multiphase Flow Simulation in Petroleum Reservoirs using the Mass Fractions as Dependent Variables", SPE 39067-MS, Latin American and Caribbean Petroleum Engineering Conference, Rio de Janeiro, Brazil.

MARCONDES, F., and Sepehrnoori, K., 2007, Unstructured Grids and an Element Based Conservative Approach for Compositional Reservoir Simulation, The 19th International Congress of Mechanical Engineering, November 5-9, Brasília, DF, Brazil.

MARCONDES, F.; Sepehrnoori, K., 2010, An Element-based Finite-Volume Method Approach for Heterogeneous and Anisotropic Compositional Reservoir Simulation, Journal of Petroleum Science and Engineering, 73, pp. 99-106.

PEACEMAN, D.W.: Fundamentals of Numerical Reservoir Simulation, Elsevier Scientific Pub. Comp., 1977.

THOMSON, J. F., Warsi Z. U. A., and Mastin, C. W., 1985 "Numerical Grid Generation –Foundation and Applications", Elsevier Sciennce Publishing Co., EUA.

6. RESPONSIBILITY NOTICE

The authors are the only responsible for the printed material included in this paper.